International Journal of Control, Automation and Systems 20(8) (2022) 2459-2473
http://dx.doi.org/10.1007/s12555-021-0643-6
ISSN:1598-6446 eISSN:2005-4092
http://www.springer.com/12555

Composite Design of Disturbance Observer and Reentry Attitude Controller: An Enhanced Finite-time Technique for Aeroservoelastic Reusable Launch Vehicles

Zhenshu Yang, Qi Mao*, Liqian Dou, Qun Zong, and Jianzhong Yang

Abstract: In this paper, we concern the reentry attitude control (RAC) scheme design for aeroservoelastic reusable launch vehicles (RLVs). The basic problem is to derive a RAC technique such that the aeroservoelastic RLV can achieve a robust tracking of the desired attitudes in a rapid way despite the existence of parameter uncertainties as well as external disturbances. Following from the elastic equations and attitude dynamics of the RLV, we formulate a control-oriented model in matched structure. Our main contribution is threefold. First, using the fast terminal sliding mode algorithm, the disturbance observers are designed to generate the estimation of uncertainties and disturbances, while can ensure the estimation errors converge to the origin within a timely fashion. Second, the finite-time super-twisting sliding mode control method and cascade-loop design are developed to incorporate into the new RAC strategy; hence it leads to a guaranteed tracking ability of the reentry attitude in a timely way. Third, a finite-time integral sliding mode filter is proposed in the control scheme such that the virtual input signal can be tackled well. Additionally, numerical simulations of a dynamic model for the RLV are implemented to demonstrate the effectiveness and performance of the developed RAC strategy and furthermore its aeroservoelastic properties.

Keywords: Disturbance observer, finite-time convergence, integral sliding mode filter, reentry attitude control, super-twisting sliding mode.

1. INTRODUCTION

The reusable launch vehicle (RLV) has gained sustained interest over the past decades, since it provides great advantages over the traditional flight vehicle in reusability, reliability, and lateral maneuverability [1]. The increasing attention in this technology is principally because of the advantages it offers. A cost-effective way of accessing the space and the ability to prompt globally high-speed delivery are the two main mission objectives for RLV. The control system design of an RLV within the reenty process, however, is a particular challenge because of the peculiar characteristic of the vehicle such as fast time-varying, strongly interactive, multivariate strongly coupling and highly nonlinear [2–5]. Beyond that, the vehicle is susceptible to various parameter uncertainties and unknown external disturbances in view of the fact that the RLV involves attitude maneuvering through a wide range of flight conditions during the reentry phase. As such, the flight vehicle is likely subject to poor flight condition and various reentry constraints. In addition to the complexity of the dynamics of reentry flight, the aeroservoelasticity problem, which results from the coupling impacts of the control system, aerodynamics forces, and structural elasticity, should be taken into consideration as well [6–8]. All these factors cause difficulty for designing reentry attitude controllers, and thus developing advanced guidance and control technologies for RLV are significant.

Despite having the aforementioned challenges, much effort has been concentrated on aeroelastic problems and control methods for RLV during the past few decades. Most early, Ricketts *et al*. have studied the aeroelasticity model of National Aerospace Plane [9]. After that, an X-30 configuration-based analytical model was proposed by Chavez and Schmidt, where the aerodynamic equations of the aerocraft forces and moments are computed under the framework of Newton collision theory [10]. In the work of [11], a hypersonic flight vehicle model was established

Manuscript received August 4, 2021; revised September 24, 2021; accepted October 7, 2021. Recommended by Associate Editor Zehui Mao under the direction of Editor Bin Jiang. This work was supported in part by the 2020-2021 Open Fund of the Key Laboratory of Civil Aviation Aircraft Airworthiness Certification Technology under Grant SH2020112704 and in part by the National Natural Science Foundation of China under Grant 61773278, Grant 61773279, Grant 61873340.

Zhenshu Yang and Jianzhong Yang are with the Key Laboratory of Civil Aviation Aircraft Airworthiness Certification Technology, Civil Aviation University of China, Tianjin 300399, China (e-mails: zhenshuyang@outlook.com, jzyang2004@126.com). Qi Mao is with the Department of Electrical Engineering, City University of Hong Kong, Kowloon, Hong Kong, China, and the School of Electrical and Information Engineering, Tianjin University, Tianjin 300072, China (e-mail: maoqi1118@tju.edu.cn). Liqian Dou and Qun Zong are with the School of Electrical and Information Engineering, Tianjin University, Tianjin 300072, China (e-mails: {douliqian,zongqun}@tju.edu.cn).
* Corresponding author.

via X-43A configuration by utilizing the Lagrange expression and the interaction of the rigid and elastic bodies were both taken into account as well. Hu *et al*. [12] have used the adaptive sliding mode control method for flexible flight vehicles with strong flexibility effects. In recent years, a dynamic surface approach was designed to robustly track the desired commands for a hypersonic vehicle in the presence of input constraints and uncertainty [13]. In [14], the trajectory planning strategy for the entire recovery process has been studied for the reusable launch vehicle, wherein the revised trajectory correction approach was designed to reduce the maximum normal aerodynamic load and enhance the vehicle's landing accuracy on the influence of wind field. Wang *et al*. [15] developed a sliding mode control algorithm in a high-order form such that the expected reference signals can be tracked well for airbreathing hypersonic vehicles. In [16], Falcoz *et al*. have designed fault detection and isolation systems on the basis of a robust model, where the interacted impacts in vehicle dynamics and the fault effects were considered during the design process. Fiorentini and Serrani [17] provided a nonlinear robust controller design for a type of hypersonic vehicle that associates with a nonminimum phase dynamic model, where the small-gain arguments were combined with adaptive control methods to construct a state-feedback controller. Zuo *et al*. [18,19] has investigated the robust fixed-time stabilization control problem for generic linear systems subject to both matched and mismatched disturbances. This leads to a novel observer-based fixed-time control technique, which was invoked to deal with this robust stabilization issue. In [20], feedback linearization was employed with disturbance observer to design a state-feedback control strategy thereby regulating the velocity and altitude for flight vehicles with constrained inputs.

At the same time, numerous attempts have been probed to develop the control laws for flight vehicles. Traditionally, gain scheduling is widely employed to tackle varying aircraft dynamics [21,22]. This approach, however, cannot be always useful when applied to the aeroservoelastic RLV because it may require wide-range flight envelop and aggressive maneuvering. As an alternative methodology, dynamic inversion has been extensively investigated over the last few decades. Although the control algorithm can avoid the tedious gain scheduling process and achieve good tracking performance, this method is not robust generally, especially in the case of parameter inaccuracies and modeling errors. Another control design method is feedback linearization with the advantage that it offers a nonlinear flight control system with a full envelope [23,24]. The main issue of this method, though, is that it requires lots of information on the RLV model. Su and Wang [25] have developed a robust hybrid optimization approach on the basis of gauss pseudospectral technique and gravitational search method to tackle the problem of e trajectory optimization for RLVs. In [26], a data-driven supplementary-based tracking control technique, was derived by using action-dependent heuristic dynamic programming method for air-breathing hypersonic vehicles; this control algorithm performs well in adaptive learning capability. To address the nonminimum phase problem, the output redefinition approach was combined with robust backstepping in the work of [27]. Under this circumstance, a synthetic output was constructed by employing the original output and the internal states to achieve stable zero dynamics, while the robust backstepping was acted on the new output.

Among a variety of control methods, the sliding mode control (SMC) technique is still one of the most popular design tools for designing a robust control law for reentry RLV. Shtessel *et al*. [28,29] have intensively explored the feasibility of sliding mode controllers for a series of RLVs. In the work of [30], a sliding mode flight control algorithm was employed for launch vehicles by constructing higher-order single and multiple loop controller accompanied with sliding mode disturbance observer. Focusing on the control problem of underactuated hypersonic vehicles with nonminimum phase structure, Wang *et al*. [31] have designed a second-order dynamic sliding-mode control algorithm, where the non-minimum phase system was separated into a minimum phase subsystem and a nonminimum phase subsystem. Subsequently, Zong *et al*. [32] have developed a quasi-continuous high-order sliding mode technique based on full state feedback for flexible spacecrafts. Nevertheless, the great majority of control laws mentioned above are derived under the worst circumstance. In the studies of [1,33–36], several intelligent control techniques like fuzzy logic system, neural control systems are employed to construct guidance strategies or attitude control schemes, which guarantees the tracking performance for the flight vehicles. As shown in [37–40], the systems that are able to be stabilized within finite time exhibit more rapid convergence rate and perform stronger anti-disturbance ability. One main constrain of most methods mentioned before, however, is that the reusable launch vehicle is deemed as a rigid-body vehicle. Specifically, the aeroservoelasticity factor [6], various parameter uncertainties as well as unknown disturbances are not considered simultaneously. Beyond that, it is noteworthy that most studies concentrate on attitude control method design, but the physical issues of flight dynamics are often neglected. In these scenarios, it is not very sufficient to verify the efficiency or tracking capability of the proposed control methodologies.

Inspired by the above-mentioned discussion, in this paper, we focus the issue of RAC scheme design for aeroservoelastic RLV with parameter uncertainties and external disturbances, with the goal to generate a performance-enhanced solution to control the RLV during the reentry phase. Compared with the previous works, the main contributions lie in the following folds.

1) The aeroservoelastic RLV model presented in this work integrates not only parameter uncertainties and external disturbances but aeroservoelastic factors. With dynamics transformation, a control-oriented model in matched structure is established.
2) A finite-time sliding mode disturbance observer (FTSMDO) is developed via the fast terminal sliding mode technique to estimate the uncertainties and disturbances. Next, a new integral sliding mode filter with finite-time convergence is constructed to deal with the virtual input signal. Incorporated the designed FTSMDOs and integral sliding mode filter, a novel finite-time RAC scheme is derived with the feature of assuring that the attitude tracking could be achieved within a finite time.
3) The finite-time stability is provided rigorously under the framework of Lyapunov stability theory. Through simulations and comparison discussions, the proposed control scheme can efficiently improve the attitude tracking performance, and the elastic coordinates as well as its derivatives converge quickly.

This paper is summarized as follows: In Section 2, we begin with several definitions and lemma. The problem formulation is provided in Section 3. After that, we move forward to develop a finite-time RAC scheme for finite-time reentry attitude control in Section 4. Section 5 provides the numerical simulations and some discussions about these results. Finally, Section 6 presents the conclusions in this work.

2. PROBLEM FORMULATION

2.1. Aeroservoelastic RLV dynamics

2.1.1 Elastic equations of motion

The fuselage elastic equation of motion can be constructed for the aeroservoelastic RLV by

$$\ddot{\eta}_i + 2\xi_i\omega_{fi}\dot{\eta}_i + \omega_{fi}^2\eta_i = N_i,\ i = 1,\ 2,\ \dots,\ n_v, \tag{1}$$

where η_i is the generalized elastic coordinate, ξ_i is the structural damping ratio, w_{fi} is the vibration frequency, N_i is the generalized modal force, and n_v denotes the number of the retained modes. Note that $n_v = 3$ is true due to the system structure of a RLV.

Remark 1: It is remarkable pointing out that the major factor causing fuselage flexibility of aerospace vehicles is the longitudinal bending [9]. As such, this leads to that the aerodynamic drag force and aerodynamic lift force are both involved with the elastic factors; analogously, the roll and pitch moments are also subject to the elastic factors.

The generalized forces N_i are described by

$$N_i = \frac{1}{2}\rho(h)v^2 S_{ref} C_{N_i}(Ma,\ h,\ \alpha,\ \eta_i,\ \delta_t), \tag{2}$$

where N_i is indirect function of Ma, h, α, η_i, δ_t (which are detailed in a minute) by a direct dependence on the generalized force coefficients C_{N_i}, $i = 1,\ 2,\ 3$.

2.1.2 Translational equations of motion

In this work, we assume that the RLV within reentry process is unpowered; it is always correct for the RLV. Beyond that, it is assumed that the atmosphere is stationary, and mass variation is negligible. The forces acting upon the aerocraft merely consider gravity and aerodynamic forces.

The mathematical model for an aeroservoelastic RLV is comprised of the translational equations of motion and the rotational equations of motion. The translational dynamics resulted from the aerodynamic forces which act upon the vehicle are given rise to the trajectory generations of the flight vehicles. The translational equations of motion are stated by

$$\dot{h} = v\sin\gamma, \tag{3}$$

$$\dot{\theta} = \frac{v\cos\gamma\sin\chi}{r_e\cos\phi}, \tag{4}$$

$$\dot{\phi} = \frac{v\cos\gamma\cos\chi}{r_e}, \tag{5}$$

$$\begin{aligned}\dot{v} = &-\frac{D}{m} - g\sin\gamma \\ &+ \Omega_e^2 r_e\cos\theta(\sin\gamma\cos\theta - \cos\gamma\sin\theta\cos\chi),\end{aligned} \tag{6}$$

$$\begin{aligned}\dot{\chi} = &\frac{1}{mv\cos\gamma}(L\sin\mu + Y\cos\mu) + \frac{v}{r_e}\cos\gamma\sin\chi\tan\theta \\ &- 2\Omega_e(\tan\gamma\cos\theta\cos\chi - \sin\theta) \\ &+ \frac{\Omega_e^2 r_e}{v\cos\gamma}\sin\theta\cos\theta\sin\chi,\end{aligned} \tag{7}$$

$$\begin{aligned}\dot{\gamma} = &\frac{1}{mv}(L\cos\mu - Y\sin\mu) - (\frac{g}{v} - \frac{v}{r_e})\cos\gamma \\ &+ 2\Omega_e\cos\theta sin\chi \\ &+ \frac{\Omega_e^2 r_e}{v}\cos\theta(\cos\gamma\cos\theta + \sin\gamma\sin\theta\cos\chi),\end{aligned} \tag{8}$$

where h denotes the altitude; θ denotes the latitude; ϕ denotes the longitude; v is the velocity; χ is the heading angle; γ is the flight path angle (FPA); m is the mass of the vehicle; r_e stands for the radial distance from Earth center to the vehicle; g is acceleration due to gravity ($g = \mu_e/r_e^2$ with μ_e being the gravity constant of the Earth); Ω_e represents the Earth rotational velocity; α, μ stand for the angle of attack (AOA), bank angle (BA). It is noteworthy that the effect of the Earth rotation can be neglected, i.e., the angular velocity Ω_e of the earth in (6)-(8) is regarded as zero. L, D, Y are the aerodynamic lift, drag and side forces acting on the flight vehicle respectively; specifically, its explicit dynamics are expressed as

$$L = \frac{1}{2}\rho(h)v^2 S_{ref} C_L(Ma, \alpha, \beta, \eta_i), \tag{9}$$

$$D = \frac{1}{2}\rho(h)v^2 S_{ref} C_D(Ma, \alpha, \beta, \eta_i), \tag{10}$$

$$Y = \frac{1}{2}\rho(h)v^2 S_{ref} C_Y(Ma, \alpha, \beta), \tag{11}$$

where $\rho(h)$ denotes the air density, S_{ref} denotes the aerodynamic reference area of the vehicle. $C_L(\cdot), C_D(\cdot)$ are the lift coefficient and drag coefficient respectively, all of which are the functions of Mach number Ma, angle of attack α, sideslip angle β and generalized elastic coordinates η_i ($i = 1, 2, 3$). $C_Y(\cdot)$ denotes the lateral coefficient that is the function of Ma, α, β. In addition, Ma is denoted by $Ma = v/v_c$, in which v_c denotes the nominal speed of sound and is assumed to not vary with altitude.

2.1.3 Rotational equations of motion

The rotational dynamics resulted from the aerodynamic moments which act upon the vehicle are utilized to develop the attitude controller. The rotational equations of motion are formulated as

$$\begin{aligned}\dot{\alpha} &= q - \tan\beta(p\cos\alpha + r\sin\alpha) \\ &\quad + \frac{1}{mv\cos\beta}(mg\cos\gamma\cos\mu - L),\end{aligned} \tag{12}$$

$$\dot{\beta} = p\sin\alpha - r\cos\alpha + \frac{1}{mv}(mg\cos\gamma\sin\mu + Y), \tag{13}$$

$$\begin{aligned}\dot{\mu} &= \sec\beta(p\cos\alpha + r\sin\alpha) \\ &\quad + \frac{1}{mv}[-mg\cos\gamma\cos\mu\tan\beta \\ &\quad + L(\tan\gamma\sin\mu + \tan\beta) + Y\tan\gamma\cos\mu\cos\beta],\end{aligned} \tag{14}$$

$$\begin{aligned}\dot{p} &= \frac{1}{I_{xx}I_{zz} - I_{xz}^2}\{I_{zz}[\bar{L} - (I_{zz} - I_{yy})qr + I_{xz}qp] \\ &\quad + I_{xz}[\bar{N} + (I_{xx} - I_{yy})qp - I_{xz}qr]\},\end{aligned} \tag{15}$$

$$\dot{q} = \frac{1}{I_{yy}}[\bar{M} - (I_{xx} - I_{zz})pr - I_{xz}(p^2 - r^2)], \tag{16}$$

$$\begin{aligned}\dot{r} &= \frac{1}{I_{xx}I_{zz} - I_{xz}^2}\{I_{xz}[\bar{L} + (I_{yy} - I_{zz})qr + I_{xz}qp] \\ &\quad + I_{xx}[\bar{N} + (I_{xx} - I_{yy})qp - I_{xz}qr]\},\end{aligned} \tag{17}$$

where p, q and r are roll, pitch and yaw angular rates, respectively; I_{xx}, I_{yy}, I_{zz}, I_{xz} denote moments of inertia and it is worth noting that the considered RLV model in this work is symmetrical with respect to its vertical plane. $\bar{L}$, $\bar{M}$ and $\bar{N}$ stand for roll, pitch and yaw moments acting upon the flight vehicle; in general, its explicit equations can be described by

$$\bar{L} = \frac{1}{2}\rho(h)\bar{b}v^2 S_{ref} C_{\bar{L}}(Ma, \alpha, \beta, \eta_i, \delta_a, \delta_f, \delta_t), \tag{18}$$

$$\bar{M} = \frac{1}{2}\rho(h)\bar{c}v^2 S_{ref} C_{\bar{M}}(Ma, \alpha, \beta, \eta_i, \delta_a, \delta_f, \delta_t), \tag{19}$$

$$\bar{N} = \frac{1}{2}\rho(h)\bar{b}v^2 S_{ref} C_{\bar{N}}(Ma, \alpha, \beta, \delta_a, \delta_f, \delta_t), \tag{20}$$

where $\bar{b}$ denote the wing span and $\bar{c}$ denote the wing mean geometric chord. $C_{\bar{L}}(\cdot)$, $C_{\bar{M}}(\cdot)$ are the roll coefficient and pitch coefficient respectively; in fact, all of these coefficients are the functions of Ma, α, β, η_i, deflection angle of aileron δ_a, deflection angle of flap δ_f, deflection angle of tail δ_t. $C_{\bar{N}}(\cdot)$ stands for yaw coefficient that is the function of Ma, α, β, δ_a, δ_f, δ_t.

2.2. Control-oriented model

The attitude dynamics for an aeroservoelastic RLV during reentry phase are able to be converted into a cascade system, described by

$$\dot{\Omega} = G_\Omega w + F_\Omega + d_\Omega, \tag{21}$$

$$\dot{w} = G_w w + F_w u + d_w, \tag{22}$$

where $\Omega = [\alpha,\ \beta,\ \mu]^T$ and $w = [p,\ q,\ r]^T$ denote the attitude angle vector and angular rate vector; $u = [\bar{L},\ \bar{M},\ \bar{N}]^T$ is the control input vector; $y = \Omega$ is the system output vector; $d_\Omega = [d_{\Omega_1},\ d_{\Omega_2},\ d_{\Omega_3}]^T \in \Re^{3\times 1}$ denotes the parameter uncertainties induced by the perturbation of aerodynamic coefficients; $d_w = [d_{w_1},\ d_{w_2},\ d_{w_3}]^T \in \Re^{3\times 1}$ denotes synthetic disturbances and $d_w = I^{-1}(d_0 - \Delta I\dot{w} - M\Delta Iw)$ in which ΔI stands for the model parameter uncertainties and $d_0 \in \Re^{3\times 1}$ for the external disturbances; $G_\Omega \in \Re^{3\times 3}$, $F_\Omega = [f_\alpha,\ f_\beta,\ f_\mu]^T \in \Re^{3\times 1}$, $G_w = -I^{-1}MI \in \Re^{3\times 3}$ and $F_w = I^{-1} \in \Re^{3\times 3}$ represent the known system function matrices provided as follows:

$$G_\Omega = \begin{bmatrix} -\cos\alpha\tan\beta & 1 & -\sin\alpha\tan\beta \\ \sin\alpha & 0 & -\cos\alpha \\ \cos\alpha\sec\beta & 0 & \sin\alpha\sec\beta \end{bmatrix}, \tag{23}$$

$$I = \begin{bmatrix} I_{xx} & -I_{xy} & -I_{xz} \\ -I_{xy} & I_{yy} & -I_{yz} \\ -I_{zx} & -I_{zy} & I_{zz} \end{bmatrix},\ M = \begin{bmatrix} 0 & -r & q \\ r & 0 & -p \\ -q & p & 0 \end{bmatrix}, \tag{24}$$

$$F_\Omega = \begin{bmatrix} \frac{1}{mv\cos\beta}(mg\cos\gamma\cos\mu - L) \\ \frac{1}{mv}(mg\cos\gamma\sin\mu + Y) \\ \frac{1}{mv}\begin{bmatrix} -mg\cos\gamma\cos\mu\tan\beta + L(\tan\beta \\ +\tan\gamma\sin\mu) + Y\tan\gamma\cos\mu\cos\beta \end{bmatrix} \end{bmatrix}. \tag{25}$$

Assumption 1: The uncertainty d_Ω and disturbance d_w are assumed to be unknown but bounded and differentiable, i.e., there exist positive constants $\bar{d}_i$ and d_i^U such that $\|d_i\| \le \bar{d}_i$, $\|d_i\|_\infty \le \bar{d}_i$, and $\|\dot{d}_i\| \le d_i^U$, $\|\dot{d}_i\|_\infty \le d_i^U$, $i = \Omega, w$.

Remark 2: It should be noted that the sideslip angle β is assumed to be in the interval of $(-90, 90)$ degrees. Considering the practical significance of (21) and (22), it is of great importance to note that the function matrixes G_Ω, G_w and F_w are nonsingular as long as the system is not at equilibrium, and bounded in this paper (which is typically correct).

2.3. Control objective

The goal is to derive a reentry attitude control strategy such that the RLV system is able to fulfill

1) The guidance commands $\Omega_d = [\alpha_d,\ \beta_d,\ \mu_d]^T$ are tracked by system output within a finite amount of time and then

$$\lim_{t\to t_f} \|\alpha-\alpha_d\| = 0,\ \lim_{t\to t_f} \|\beta-\beta_d\| = 0,$$
$$\lim_{t\to t_f} \|\mu-\mu_d\| = 0, \tag{26}$$

where t_f is a finite time.

2) A cascade-loop design of reentry attitude control for aeroservoelastic RLV is constructed despite having uncertainties and disturbances even if d_Ω and d_w are not known.
3) The convergence of generalized elastic coordinate η_i and its derivative $\dot{\eta}_i$ can be guaranteed.

3. FINITE-TIME RAC SCHEME DESIGN

The finite-time RAC scheme is the main concern of our work. It aims at outputting the actual attitude angles that is necessary to track the desired attitude angles and additionally dealing with the system uncertainties and disturbances. As a consequence, two main issues are investigated in the subsequent sections. The first problem is to design FTSMDO, in other words, we seek to derive disturbance observers based on the fast terminal sliding mode technique to counteract uncertainties and disturbances. On the other hand, the subsequent focus is constructing the reentry attitude controller: determine the outer-loop controller and inner-loop controller, using the finite-time super-twisting sliding mode algorithm.

3.1. The design of FTSMDO

In this section, the system uncertainty d_Ω and disturbance d_w will be estimated via the designed FTSMDO in finite time. Towards this goal, the theorem is provided as follows.

Theorem 1: Consider the RLV system described by (21), (22) under Assumption 1, and define the disturbance observer estimation errors as $A_\Omega = Z_\Omega - \Omega$ and $A_w = Z_w - w$, where Z_Ω, Z_w denote the estimation states of Ω, w. If the disturbance observers based on fast terminal sliding mode method are constructed as

$$\begin{aligned}\hat{d}_\Omega = &-\alpha_\Omega \frac{A_\Omega}{\|A_\Omega\|} - k_{\Omega 1} sig^{p_\Omega/q_\Omega}(A_\Omega)\\ &- k_{\Omega 2} sig^{q_\Omega/p_\Omega}(A_\Omega),\end{aligned} \tag{27}$$

$$\begin{aligned}\hat{d}_w = &-\alpha_w \frac{A_w}{\|A_w\|} - k_{w1} sig^{p_w/q_w}(A_w)\\ &- k_{w2} sig^{q_w/p_w}(A_w),\end{aligned} \tag{28}$$

under the condition

$$\begin{cases}\alpha_\Omega \ge \bar{d}_\Omega,\ k_{\Omega 1} > 0,\ k_{\Omega 2} > 0,\ p_\Omega > q_\Omega > 0,\\ \alpha_w \ge \bar{d}_w,\ k_{w1} > 0,\ k_{w2} > 0,\ p_w > q_w > 0,\end{cases} \tag{29}$$

where the states Z_Ω and Z_w are determined as

$$\begin{aligned}\dot{Z}_\Omega = &-\alpha_\Omega \frac{A_\Omega}{\|A_\Omega\|} - k_{\Omega 1} sig^{p_\Omega/q_\Omega}(A_\Omega)\\ &- k_{\Omega 2} sig^{q_\Omega/p_\Omega}(A_\Omega) + G_\Omega w + F_\Omega,\end{aligned} \tag{30}$$

$$\begin{aligned}\dot{Z}_w = &-\alpha_w \frac{A_w}{\|A_w\|} - k_{w1} sig^{p_w/q_w}(A_w)\\ &- k_{w2} sig^{q_w/p_w}(A_w) + G_w w + F_w u,\end{aligned} \tag{31}$$

then the estimated values $\hat{d}_\Omega$ and $\hat{d}_w$ can both converge to real uncertainty d_Ω and disturbance d_w within finite time.

Proof: Taking the derivative of A_Ω, we are led to

$$\begin{aligned}\dot{A}_\Omega &= \dot{Z}_\Omega - \dot{\Omega}\\ &= -\alpha_\Omega \frac{A_\Omega}{\|A_\Omega\|} - k_{\Omega 1} sig^{p_\Omega/q_\Omega}(A_\Omega)\\ &\quad - k_{\Omega 2} sig^{q_\Omega/p_\Omega}(A_\Omega) - d_\Omega.\end{aligned} \tag{32}$$

Choose the Lyapunov function candidate as

$$V_\Omega = \frac{1}{2} A_\Omega^T A_\Omega. \tag{33}$$

Clearly V_Ω in (33) denotes a positive definite and unbounded function. After that, the derivative of V_Ω for $A_\Omega \neq 0$ is described by

$$\begin{aligned}\dot{V}_\Omega = &-\sum_{j=1}^{3}\left(k_{\Omega 1}|A_{\Omega j}|^{p_\Omega/q_\Omega+1} + k_{\Omega 2}|A_{\Omega j}|^{q_\Omega/p_\Omega+1}\right)\\ &- \alpha_\Omega \|A_\Omega\| - A_\Omega^T d_\Omega.\end{aligned} \tag{34}$$

Invoking the Cauchy-Schwarz inequality to deal with the inner-product terms, it gives

$$\begin{aligned}\dot{V}_\Omega \le &-\sum_{j=1}^{3}\left(k_{\Omega 1}|A_{\Omega j}|^{p_\Omega/q_\Omega+1} + k_{\Omega 2}|A_{\Omega j}|^{q_\Omega/p_\Omega+1}\right)\\ &- \alpha_\Omega \|A_\Omega\| + \left\|A_\Omega^T\right\| \|d_\Omega\|\\ \le &-\sum_{j=1}^{3}\left(k_{\Omega 1}|A_{\Omega j}|^{p_\Omega/q_\Omega+1} + k_{\Omega 2}|A_{\Omega j}|^{q_\Omega/p_\Omega+1}\right)\\ \le &-k_{\Omega 2}\sum_{j=1}^{3}|A_{\Omega j}|^{q_\Omega/p_\Omega+1}.\end{aligned} \tag{35}$$

In view of Lemma 2 in [41] and $0 < q_\Omega/p_\Omega + 1 < 2$, the derivative of the Lyapunov function can be transformed into

$$\dot{V}_\Omega \le -k_{\Omega 2}\left(\sum_{j=1}^{3} A_{\Omega j}^2\right)^{\frac{q_\Omega/p_\Omega+1}{2}}$$

$$= -2^{\frac{q_\Omega/p_\Omega+1}{2}} k_{\Omega 2} V_\Omega^{\frac{q_\Omega/p_\Omega+1}{2}}. \tag{36}$$

Consequently, it follows from Lemma 1 and (36) that the estimation error A_Ω converges to zero within finite time, where $t_{f\Omega} \le \frac{V_\Omega^{\frac{1-q_\Omega/p_\Omega}{2}}}{2^{\frac{q_\Omega/p_\Omega+1}{2}} k_{\Omega 2}\left(\frac{1-q_\Omega/p_\Omega}{2}\right)}$, and then $V_\Omega = 0$ when $A_\Omega = 0$. After that, it has $\dot{A}_\Omega = \dot{Z}_\Omega - \dot{\Omega} = 0$, which implicates that the disturbance observer $\hat{d}_\Omega$ can estimate real uncertainty d_Ω in finite time. Applying the similar proof for angular rate subsystem, it can be concluded that the disturbance observer $\hat{d}_w$ can estimate real disturbance d_w within finite time, where $t_{fw} \le \frac{V_w^{\frac{1-q_w/p_w}{2}}}{2^{\frac{q_w/p_w+1}{2}} k_{w2}\left(\frac{1-q_w/p_w}{2}\right)}$. This completes the proof. □

Remark 3: The fast terminal sliding mode technique incorporated to the design of FTSMDO assures that the disturbance observer converges to equilibrium point in a fast speed. Compared with the existing sliding mode disturbance observers [42], the developed FTSMDO can insure the finite time convergence of disturbance estimation error.

3.2. The design of reentry attitude controller

3.2.1 Control law for attitude angle subsystem

With respect to (21), denote the attitude tracking error as $E_\Omega = [E_{\Omega 1}, E_{\Omega 2}, E_{\Omega 3}]^T = \Omega - \Omega_d$, and a new fast sliding mode surface is defined as

$$S_\Omega = l_{\Omega 0} E_\Omega + l_{\Omega 1} sig^{\frac{m_\Omega + n_\Omega}{n_\Omega}}(E_\Omega) + l_{\Omega 2} sig^{\frac{n_\Omega + m_\Omega}{m_\Omega}}(E_\Omega), \tag{37}$$

where $l_{\Omega 0}, l_{\Omega 1}, l_{\Omega 2} > 0$ and $m_\Omega > n_\Omega > 0$ are the user-designed constants.

A multivariable super-twisting algorithm is employed to construct the reaching law for (37) as

$$\begin{cases} \dot{S}_\Omega = -\lambda_{\Omega 1} S_\Omega - \lambda_{\Omega 2} S_\Omega / \|S_\Omega\|^{1/2} + z_\Omega, \\ \dot{z}_\Omega = -\lambda_{\Omega 3} S_\Omega - \lambda_{\Omega 4} S_\Omega / \|S_\Omega\|, \end{cases} \tag{38}$$

where $\lambda_{\Omega 1}$, $\lambda_{\Omega 2}$, $\lambda_{\Omega 3}$, $\lambda_{\Omega 4}$ are positive constants.

Theorem 2: Consider attitude angle subsystem (21) satisfying Assumption 1. If the virtual control law is developed as

$$\begin{cases} \bar{w}_d = \dfrac{1}{l_{\Omega 0}} G_\Omega^{-1} \begin{pmatrix} -\frac{m_\Omega}{n_\Omega} l_{\Omega 1} diag\left[|E_{\Omega i}|^{\frac{m_\Omega}{n_\Omega}}\right]_{3\times 3} \dot{E}_\Omega \\ -\frac{n_\Omega}{m_\Omega} l_{\Omega 2} diag\left[|E_{\Omega i}|^{\frac{n_\Omega}{m_\Omega}}\right]_{3\times 3} \dot{E}_\Omega \\ -\lambda_{\Omega 1} S_\Omega - \lambda_{\Omega 2} S_\Omega / \|S_\Omega\|^{1/2} \\ + z_\Omega - l_{\Omega 0}\left(F_\Omega + \hat{d}_\Omega - \dot{\Omega}_d\right) \end{pmatrix}, \\ \dot{z}_\Omega = -\lambda_{\Omega 3} S_\Omega - \lambda_{\Omega 4} S_\Omega / \|S_\Omega\|, \end{cases} \tag{39}$$

under the condition

$$\begin{cases} \lambda_{\Omega 1} > 0, \lambda_{\Omega 2} > (2B_\Omega)^{1/2}, \\ \lambda_{\Omega 3} > \dfrac{\left(3\lambda_{\Omega 1}\lambda_{\Omega 2}^2 + 6\lambda_{\Omega 1} B_\Omega\right)^2}{\lambda_{\Omega 2}^2 \lambda_{\Omega 4} - 3B_\Omega \lambda_{\Omega 2}^2 - 2B_\Omega^2} + 2\lambda_{\Omega 1}^2, \\ \lambda_{\Omega 4} > \max\left\{3B_\Omega + \dfrac{2B_\Omega^2}{\lambda_{\Omega 2}^2}, \dfrac{-2\lambda_{\Omega 1}\lambda_{\Omega 2}^2 + \lambda_{\Omega 1} B_\Omega}{\lambda_{\Omega 1}}\right\}, \end{cases} \tag{40}$$

where $\hat{d}_\Omega$ is obtained using FTSMDO proposed in Theorem 1, then the developed control law guarantees that tracking error E_Ω is steered to zero in finite time.

Proof: Taking the derivative of (37) and invoking (21) yields

$$\begin{aligned} &\dot{S}_\Omega = -\lambda_{\Omega 1} S_\Omega - \lambda_{\Omega 2} S_\Omega / \|S_\Omega\|^{1/2} + z_\Omega + \tilde{d}_\Omega, \\ &\dot{z}_\Omega = -\lambda_{\Omega 3} S_\Omega - \lambda_{\Omega 4} S_\Omega / \|S_\Omega\|, \end{aligned} \tag{41}$$

where $\tilde{d}_\Omega = d_\Omega - \hat{d}_\Omega$. Denote the auxiliary variable as $\varpi_\Omega = z_\Omega + \tilde{d}_\Omega$, then (41) can be rewritten as

$$\begin{aligned} &\dot{S}_\Omega = -\lambda_{\Omega 1} S_\Omega - \lambda_{\Omega 2} S_\Omega / \|S_\Omega\|^{1/2} + \varpi_\Omega, \\ &\dot{\varpi}_\Omega = -\lambda_{\Omega 3} S_\Omega - \lambda_{\Omega 4} S_\Omega / \|S_\Omega\| + \dot{\tilde{d}}_\Omega. \end{aligned} \tag{42}$$

It follows from Theorem 1 and Assumption 1 that d_Ω, $\dot{d}_\Omega$ and $\hat{d}_\Omega$, $\dot{\hat{d}}_\Omega$ are bounded. Consequently, it is rational to assume that $\tilde{d}_\Omega$ and its derivative $\dot{\tilde{d}}_\Omega$ are bounded as well by using Cauchy-Schwarz inequality, and suppose that $\|\tilde{d}_\Omega\| \le d_\Omega^U$ with the scalar bound $d_\Omega^U > 0$ and $\upsilon_\Omega = \dot{\tilde{d}}_\Omega$ satisfying $\|\upsilon\| \le B_\Omega$ with the scalar bound B_Ω. In a similar way, it is available to assume that $\|\tilde{d}_w\| \le d_w^U$ with the scalar bound $d_w^U > 0$ and $\upsilon_w = \dot{\tilde{d}}_w$ satisfying $\|\upsilon\| \le B_w$ with the scalar bound B_w.

The proof of Theorem 2 is equivalent to validating that E_Ω can converge to zero in a limited time. Towards this aim, the Lyapunov function candidate is selected as follows:

$$W_\Omega = \lambda_{\Omega 3} S_\Omega^T S_\Omega + 2\lambda_{\Omega 4}\|S_\Omega\| + \frac{1}{2}\varpi_\Omega^T \varpi_\Omega + \frac{1}{2}\tau_\Omega^T \tau_\Omega, \tag{43}$$

where $\tau_\Omega = \lambda_{\Omega 1} S_\Omega + \lambda_{\Omega 2} S_\Omega / \|S_\Omega\|^{1/2} - \varpi_\Omega$.

Taking the derivative of W_Ω in (43), and substituting (42) into it, $\dot{W}_\Omega$ can be rewritten as

$$\begin{aligned} \dot{W}_\Omega = &-\left(\frac{1}{2}\lambda_{\Omega 2}^3 + \lambda_{\Omega 2}\lambda_{\Omega 4}\right)\|S_\Omega\|^{1/2} - \lambda_{\Omega 2}\frac{S_\Omega^T \upsilon_\Omega}{\|S_\Omega\|^{1/2}} \\ &- \left(2\lambda_{\Omega 1}\lambda_{\Omega 2}^2 + \lambda_{\Omega 1}\lambda_{\Omega 4}\right)\|S_\Omega\| + \lambda_{\Omega 2}^2 \frac{\varpi_\Omega^T S_\Omega}{\|S_\Omega\|} \\ &- \lambda_{\Omega 1} S_\Omega^T \upsilon_\Omega - \left(\frac{5}{2}\lambda_{\Omega 1}^2 \lambda_{\Omega 2} + \lambda_{\Omega 2}\lambda_{\Omega 3}\right)\|S_\Omega\|^{3/2} \\ &- \lambda_{\Omega 2}\frac{\|\varpi_\Omega\|^2}{\|S_\Omega\|^{1/2}} + 2\varpi_\Omega^T \upsilon_\Omega - \left(\lambda_{\Omega 1}^3 + \lambda_{\Omega 1}\lambda_{\Omega 3}\right)\|S_\Omega\|^2 \\ &+ 3\lambda_{\Omega 1}\lambda_{\Omega 2}\frac{S_\Omega^T \varpi_\Omega}{\|S_\Omega\|^{1/2}} + \frac{1}{2}\lambda_{\Omega 2}\frac{\varpi_\Omega^T S_\Omega S_\Omega^T \varpi_\Omega}{\|S_\Omega\|^{5/2}} \end{aligned}$$

$$+2\lambda_{\Omega 1}^2 S_\Omega^T \varpi_\Omega - \lambda_{\Omega 1}\|\varpi_\Omega\|^2. \tag{44}$$

Applying the Cauchy-Schwarz inequality on the inner product terms associated with the υ_Ω bounds, $\dot{W}_\Omega$ satisfies

$$\begin{aligned}\dot{W}_\Omega \leq & -\left(\frac{1}{2}\lambda_{\Omega 2}^3+\lambda_{\Omega 2}\lambda_{\Omega 4}\right)\|S_\Omega\|^{1/2}+\frac{\lambda_{\Omega 2}\|\varpi_\Omega\|^2}{2\|S_\Omega\|^{1/2}}\\ & -\left(2\lambda_{\Omega 1}\lambda_{\Omega 2}^2+\lambda_{\Omega 1}\lambda_{\Omega 4}\right)\|S_\Omega\|+2\lambda_{\Omega 1}^2\|\varpi_\Omega\|\|S_\Omega\|\\ & -\left(\frac{5}{2}\lambda_{\Omega 1}^2\lambda_{\Omega 2}+\lambda_{\Omega 2}\lambda_{\Omega 3}\right)\|S_\Omega\|^{3/2}\\ & +\lambda_{\Omega 2}B_\Omega\|S_\Omega\|^{1/2}+3\lambda_{\Omega 1}\lambda_{\Omega 2}\|\varpi_\Omega\|\|S_\Omega\|^{1/2}\\ & -\lambda_{\Omega 1}\|\varpi_\Omega\|^2+\lambda_{\Omega 2}^2\|\varpi_\Omega\|\\ & -\left(\lambda_{\Omega 1}^3+\lambda_{\Omega 1}\lambda_{\Omega 3}\right)\|S_\Omega\|^2\\ & +\lambda_{\Omega 1}B_\Omega\|S_\Omega\|+2B_\Omega\|\varpi_\Omega\|. \end{aligned}\tag{45}$$

For ease of Lyapunov analysis, the vector $\xi=[\xi_1,\ \xi_2,\ \xi_3]^T$ with $\xi_1=\|S_\Omega\|^{1/2}$, $\xi_2=\|S_\Omega\|$, $\xi_3=\|\varpi_\Omega\|$ is introduced. Then the derivative of the Lyapunov function in (43) can be further transformed into

$$\dot{W}_\Omega \leq -\left(\lambda_{\Omega 1}\xi^T\Xi_{\Omega 1}\xi+\lambda_{\Omega 2}\frac{1}{\|S_\Omega\|^{1/2}}\xi^T\Xi_{\Omega 2}\xi\right), \tag{46}$$

with

$$\Xi_{\Omega 1}=\begin{bmatrix}2\lambda_{\Omega 2}^2+\lambda_{\Omega 4}-B_\Omega & 0 & 0\\ 0 & \lambda_{\Omega 1}^2+\lambda_{\Omega 3} & -\lambda_{\Omega 1}\\ 0 & -\lambda_{\Omega 1} & -1\end{bmatrix},$$

$$\Xi_{\Omega 2}=\begin{bmatrix}\frac{1}{2}\lambda_{\Omega 2}^2+\lambda_{\Omega 4}-B_\Omega & 0 & -\frac{1}{2}\lambda_{\Omega 2}-\frac{B_\Omega}{\lambda_{\Omega 2}}\\ 0 & \frac{5}{2}\lambda_{\Omega 1}^2+\lambda_{\Omega 3} & -\frac{3}{2}\lambda_{\Omega 1}\\ -\frac{1}{2}\lambda_{\Omega 2}-\frac{B_\Omega}{\lambda_{\Omega 2}} & -\frac{3}{2}\lambda_{\Omega 1} & \frac{1}{2}\end{bmatrix}.$$

It follows from Theorem 2 that symmetric matrices $\Xi_{\Omega 1}$ and $\Xi_{\Omega 2}$ are positive definite under condition (40). Using the positive matrices $\Xi_{\Omega 1}$, $\Xi_{\Omega 2}$ provided above and Rayleigh's inequality, $\dot{W}_\Omega$ satisfies the inequality

$$\dot{W}_\Omega \leq -\lambda_{\Omega 2}\frac{\xi^T\Xi_2\xi}{\|S_\Omega\|^{1/2}} \leq -\lambda_{\Omega 2}\lambda_{\min}(\Xi_2)\frac{\|\xi\|^2}{\|S_\Omega\|^{1/2}}. \tag{47}$$

A new vector is defined as $\vartheta=[S_\Omega/\|S_\Omega\|^{1/2},\ S_\Omega,\ \varpi_\Omega]^T$, where it is noted that $\forall S_\Omega,\ \varpi_\Omega\in\Re^{3\times 1}$, $\|\vartheta\|=\|\xi\|$. Then, $\dot{W}_\Omega$ in (47) can be expressed as $\dot{W}_\Omega \leq -\lambda_{\Omega 2}\lambda_{\min}(\Xi_2)\frac{\|\vartheta\|^2}{\|S_\Omega\|^{1/2}}$. On the basis of the result in [43], the Lyapunov function (43) can be stated as $W_\Omega=\vartheta^T Q\vartheta$, where $Q\in\Re^{3\times 3}$ is a symmetric positive definite matrix. Similarly, by using Rayleigh's inequality, we have $W_\Omega \leq \lambda_{\max}(Q)\|\vartheta\|^2$. As such, the following inequality holds

$$\dot{W}_\Omega \leq -\frac{\lambda_{\Omega 2}\lambda_{\min}(\Xi_2)}{\lambda_{\max}(Q)}\frac{1}{\|S_\Omega\|^{1/2}}W_\Omega. \tag{48}$$

Since $W_\Omega^{1/2}>(\lambda_{\min}(Q))^{1/2}\|S_\Omega\|^{1/2}$, it yields that

$$\dot{W}_\Omega \leq -\rho_\Omega W_\Omega^{1/2}, \tag{49}$$

where $\rho_\Omega=\frac{\lambda_{\Omega 2}\lambda_{\min}(\Xi_2)(\lambda_{\min}(Q))^{1/2}}{\lambda_{\max}(Q)}$. In view of Lemma 1, it can be observed that S_Ω and its derivative $\dot{S}_\Omega$ can converge to zero in finite time t_Ω if the positive parameters $\lambda_{\Omega i}$ ($i=1,\ 2,\ 3,\ 4$) fulfilling the condition (40) are chosen appropriately, where $t_\Omega \leq \frac{2W_\Omega^{1/2}(0)}{\rho_\Omega}$.

After that, the convergence property of the tracking error E_Ω will be discussed. When S_Ω and its derivative $\dot{S}_\Omega$ converge to zero, it follows from the fast sliding mode surface designed in (37) that

$$\begin{cases}0=l_{\Omega 0}E_\Omega+l_{\Omega 1}sig^{\frac{m_\Omega+n_\Omega}{n_\Omega}}(E_\Omega)+l_{\Omega 2}sig^{\frac{n_\Omega+m_\Omega}{m_\Omega}}(E_\Omega),\\ 0=l_{\Omega 0}\dot{E}_\Omega+\dfrac{m_\Omega}{n_\Omega}l_{\Omega 1}diag\left[|E_{\Omega i}|^{\frac{m_\Omega}{n_\Omega}}\right]_{3\times 3}\dot{E}_\Omega\\ \quad +\dfrac{n_\Omega}{m_\Omega}l_{\Omega 2}diag\left[|E_{\Omega i}|^{\frac{n_\Omega}{m_\Omega}}\right]_{3\times 3}\dot{E}_\Omega.\end{cases} \tag{50}$$

Since $l_{\Omega 0}, l_{\Omega 1}, l_{\Omega 2}, m_\Omega, n_\Omega$ are the positve parameters, thus it can be concluded that E_Ω, $\dot{E}_\Omega$ are equal to zero as seen in (50) if S_Ω, $\dot{S}_\Omega$ converge to zero. Finally, the tracking error E_Ω converges to zero within finite time t_Ω. This completes the proof. □

3.2.2 Finite-time integral sliding mode filter

The control law in (39) is regarded as a virtual control signal to the angular rate (inner-loop) subsystem. However, it is not easy to obtain its accurate derivative due to the parameter uncertainties. Meanwhile, the problem of over-parameterization may occur as the steps increase. Accordingly, a finite-time integral sliding mode filter is proposed to deal with the derivative signal $\dot{\bar{w}}_d$.

Assumption 2: Due to the physical limitations for aeroservoelastic RLVs, it is rational to assume that $\bar{w}_d$ and $\dot{\bar{w}}_d$, $\dot{\psi}_{w1}$ and $\ddot{\psi}_{w1}$ are bounded, i.e., there exist positive constants ϖ^U, ϖ_d^U, ψ^U, ψ_d^U such that $\|\bar{w}_d\| \leq \|\bar{w}_d\|_{\max} \leq \varpi^U$, $\|\dot{\bar{w}}_d\| \leq \|\dot{\bar{w}}_d\|_{\max} \leq \varpi_d^U$, $\|\dot{\psi}_{w1}\| \leq \psi^U$, $\|\ddot{\psi}_{w1}\| \leq \psi_d^U$ hold.

Theorem 3: Consider the virtual control law $\bar{w}_d$ satisfying Assumption 2. If the integral sliding mode filter is designed as

$$\begin{cases}\dot{\psi}_{w1}=-\dfrac{\kappa_{w1}(\psi_{w1}-\bar{w}_d)}{\|\psi_{w1}-\bar{w}_d\|^{1/2}+\sigma_{w1}}-\dfrac{\psi_{w1}-\bar{w}_d}{\mu_{f1}},\\ \dot{\psi}_{w2}=-\dfrac{\kappa_{w2}(\psi_{w2}-\psi_{w1})}{\|\psi_{w2}-\psi_{w1}\|^{1/2}+\sigma_{w2}}-\dfrac{\psi_{w2}-\psi_{w1}}{\mu_{f2}},\end{cases} \tag{51}$$

under the condition

$$\begin{cases}\mu_{f1}>0,\ \sigma_{w1}>0,\ \kappa_{w1}=\beta_{w1}\varpi_d^U>0,\\ \mu_{f2}>0,\ \sigma_{w2}>0,\ \kappa_{w2}=\beta_{w2}\psi_d^U>0,\\ 1-\dfrac{\sigma_{w1}+1/\beta_{w1}}{\|e_{f1}\|^{1/2}/\beta_{w1}}>0,\ 1-\dfrac{\sigma_{w2}+1/\beta_{w2}}{\|e_{f2}\|^{1/2}/\beta_{w2}}>0,\end{cases} \tag{52}$$

where $\bar{w}_d = [p_d,\, q_d,\, _d r]^T$ is the desired angular rate, μ_{f1}, μ_{f2} denote the time constants of the filter, σ_{w1}, σ_{w2} are the very small constants, and $\beta_{w1},\, \beta_{w2} > 0$ are the user-designed constants, then the filter output ψ_{w1} is able to converge to $\bar{w}_d$ in finite time.

Proof: Define the filter estimation errors as $e_{f1} = \psi_{w1} - \bar{w}_d$, $e_{f2} = \psi_{w1} - \dot{\psi}_{w1}$. And the derivatives of filter estimation errors are stated as

$$\begin{aligned} \dot{e}_{f1} &= -\frac{\kappa_{w1} e_{f1}}{\|e_{f1}\|^{1/2} + \sigma_{w1}} - \frac{e_{f1}}{\mu_{f1}} - \dot{\bar{w}}_d, \\ \dot{e}_{f2} &= -\frac{\kappa_{w2} e_{f2}}{\|e_{f2}\|^{1/2} + \sigma_{w2}} - \frac{e_{f2}}{\mu_{f2}} - \ddot{\psi}_{w1}. \end{aligned} \tag{53}$$

The Lyapunov function candidate for the subsystem (21) is selected as

$$V_F = V_{f1} + V_{f2}, \tag{54}$$

with $V_{f1} = \frac{1}{2} e_{f1}^T e_{f1}, V_{f2} = \frac{1}{2} e_{f2}^T e_{f2}$.
Calculating the time derivative of V_{f1} gives

$$\begin{aligned} \dot{V}_{f1} =& -\kappa_{w1} \frac{e_{f1}^T e_{f1}}{\|e_{f1}\|^{1/2} + \sigma_{w1}} - \frac{e_{f1}^T e_{f1}}{\mu_{f1}} - e_{f1}^T \dot{\bar{w}}_d \\ =& -\kappa_{w1} \frac{e_{f1}^T e_{f1} - \sigma_{w1}^4 + \sigma_{w1}^4}{\|e_{f1}\|^{1/2} + \sigma_{w1}} - \frac{e_{f1}^T e_{f1}}{\mu_{f1}} - e_{f1}^T \dot{\bar{w}}_d \\ \le& -\kappa_{w1} \left(\|e_{f1}\| + \sigma_{w1}^2\right) \left(\|e_{f1}\|^{1/2} - \sigma_{w1}\right) \\ & - e_{f1}^T \dot{\bar{w}}_d \\ \le& -\kappa_{w1} \|e_{f1}\|^{3/2} + \kappa_{w1} \sigma_{w1} \|e_{f1}\| + \kappa_{w1} \sigma_{w1}^3 \\ & + \|e_{f1}\| \|\dot{\bar{w}}_d\|. \end{aligned} \tag{55}$$

It is noted that the parameter $0 < \sigma_{w1} \ll 1$ thereby leading to $\kappa_{w1} \sigma_{w1}^3$, and then it has

$$\dot{V}_{f1} \le -\kappa_{w1} \|e_{f1}\|^{3/2} + \kappa_{w1} \sigma_{w1} \|e_{f1}\| + \|e_{f1}\| \|\dot{\bar{w}}_d\|. \tag{56}$$

Note the fact that Assumption 2 and condition (52). Thus, the derivative of V_{f1} satisfies the inequality as follows:

$$\begin{aligned} \dot{V}_{f1} &\le -\varpi_d^U \beta_{w1} \left(\|e_{f1}\|^{3/2} - \sigma_{w1} \|e_{f1}\| - \|e_{f1}\| / \beta_{w1}\right) \\ &\le -m_{f1} V_{f1}^{3/4}, \end{aligned} \tag{57}$$

where $m_{f1} = \varpi_d^U \beta_{w1} \left(1 - \frac{\sigma_{w1} + 1/\beta_{w1}}{V_{f1}^{1/4}/\beta_{w1}}\right) > 0$. Similarly, following the same arguments yields

$$\dot{V}_{f2} \le -\psi_d^U \beta_{w2} \left(1 - \frac{\sigma_{w2} + 1/\beta_{w2}}{V_{f2}^{1/4}/\beta_{w2}}\right) V_{f2}^{3/4}, \tag{58}$$

where $m_{f2} = \psi_d^U \beta_{w2} \left(1 - \frac{\sigma_{w2} + 1/\beta_{w2}}{V_{f2}^{1/4}/\beta_{w2}}\right) > 0$.

Finally, it can be obtained that

$$\dot{V}_F \le -m_F (V_{f1} + V_{f2})^{1/2} = -m_F V_F^{1/2}, \tag{59}$$

where $m_F = \min\{m_{f1}, m_{f2}\}$. Applying Lemma 1, it is easily found that filter output ψ_{w1} can converge to virtual control signal $\bar{w}_d$ in finite time t_F(where $t_F \le 2V_F^{1/2}(x)/m_F$). This completes the proof. □

Remark 4: It is worth pointing out that the designed filter for virtual input signal can guarantee that the noise or chatter is not directly brought in the propagation channel to its derivative, and the computation of the derivative of the virtual input signal can be facilitated. Compared with the existing results, the developed integral sliding mode filter makes the estimation error converge to zero within finite time.

3.2.3 Control law for angular rate subsystem

For the angular rate subsystem (22), the angular rate tracking error is defined as $E_w = [E_{w1}, E_{w2}, E_{w3}]^T = w - \psi_{w1}$. A new fast sliding mode surface of this subsystem is given as

$$S_w = l_{w0} E_w + l_{w1} sig^{\frac{m_w + n_w}{n_w}}(E_w) + l_{w2} sig^{\frac{n_w + m_w}{m_w}}(E_w), \tag{60}$$

where l_{w0}, l_{w1}, $l_{w2} > 0$, and $m_w > n_w > 0$ denote the user-designed constants.

Similarly, a multivariable super-twisting method is incorporated to develop the sliding mode reaching law for (60) as

$$\begin{cases} \dot{S}_w = -\lambda_{w1} S_w - \lambda_{w2} S_w / \|S_w\|^{1/2} + z_w, \\ \dot{z}_w = -\lambda_{w3} S_w - \lambda_{w4} S_w / \|S_w\|, \end{cases} \tag{61}$$

where λ_{w1}, λ_{w2}, λ_{w3}, λ_{w4} are positive constants. The following theorem is available for the angular rate subsystem.

Theorem 4: Consider angular rate subsystem (22) fulfilling Assumptions 1 and 2. If the actual control law is presented as

$$\begin{cases} u = \dfrac{1}{l_{w0}} F_w^{-1} \begin{pmatrix} -\frac{m_w}{n_w} l_{w1} diag\left[|E_{wi}|^{\frac{m_w}{n_w}}\right]_{3\times 3} \dot{E}_w \\ -\frac{n_w}{m_w} l_{w2} diag\left[|E_{wi}|^{\frac{n_w}{m_w}}\right]_{3\times 3} \dot{E}_w \\ -\lambda_{w1} S_w - \lambda_{w2} S_w / \|S_w\|^{1/2} \\ + z_w - l_{w0}\left(G_w w + \hat{d}_w - \dot{\psi}_{w1}\right) \end{pmatrix}, \\ \dot{z}_w = -\lambda_{w3} S_w - \lambda_{w4} S_w / \|S_w\|, \end{cases} \tag{62}$$

under the condition

$$\begin{cases} \lambda_{w1} > 0, \lambda_{w2} > (2B_w)^{1/2}, \\ \lambda_{w3} > \dfrac{\left(3\lambda_{w1}\lambda_{w2}^2 + 6\lambda_{w1} B_w\right)^2}{\lambda_{w2}^2 \lambda_{w4} - 3B_w \lambda_{w2}^2 - 2B_w^2} + 2\lambda_{w1}^2, \\ \lambda_{w4} > \max\left\{3B_w + \dfrac{2B_w^2}{\lambda_{w2}^2}, \dfrac{-2\lambda_{w1}\lambda_{w2}^2 + \lambda_{w1} B_w}{\lambda_{w1}}\right\}, \end{cases} \tag{63}$$

where $\hat{d}_w$ is derived based on FTSMDO technique, then the proposed control law can assure that tracking error E_w converges to zero in finite time.

Following the analogous proof in Theorem 2, we can conclude that S_w and its derivative $\dot{S}_w$ are able to converge to zero in a timely fashion and further enforce E_w, $\dot{E}_w$ converge to zero within a timely manner as well.

Remark 5: In the light of the multiple-timescale separation principle, it is noted that the controllers of the attitude angle and angular rate subsystems can be constructed separately, where the finite-time stability of the overall control system is then guaranteed.

4. NUMERICAL SIMULATIONS

4.1. Parameter setting

The RLV parameters used in the numerical simulations are provided as follows: $I_{xx} = 434,270$ slug·ft^2, $I_{xz} = 17,880$ slug·ft^2, $I_{yy} = 961,220$ slug·ft^2, $I_{zz} = 1,131,541$ slug·ft^2 and $I_{xy} = I_{yz} = 0$ slug·ft^2. The initial flight conditions of the reentry RLV is given as: $\alpha_0 = 5.62$ deg, $\beta_0 = 28.65$ deg, $\mu_0 = -5.46$ deg and $p_0 = q_0 = r_0 = 0$ deg/s. For the sake of better illustrating the efficiency of the developed algorithm, the desired command signals are chosen as Sine function, which is typically rational. In addition, the parameter uncertainty d_Ω and synthetic disturbance d_w is taken into consideration as well to demonstrate the attitude tracking performance of the proposed method, as seen in [2]. The uncertainty d_Ω is attributed to the perturbation of the nominal nonlinear function F_Ω, i.e., $d_\Omega = \pm 10\% F_\Omega$, while the disturbances is set as

$$d_w = 10^6 \times \begin{bmatrix} (1+\sin(\pi t/100)+\sin(\pi t/125))/I_{xx} \\ (1+\sin(\pi t/100)+\cos(\pi t/125))/I_{yy} \\ (1+\cos(\pi t/100)+\sin(\pi t/125))/I_{zz} \end{bmatrix}.$$

The designed controller parameters are selected as follows: $l_{\Omega 0} = 0.95$, $l_{\Omega 1} = 2$, $l_{\Omega 2} = 1$, $m_\Omega = 1.5$, $n_\Omega = 0.6$, $\lambda_{\Omega 1} = 3.6$, $\lambda_{\Omega 2} = 2$, $\lambda_{\Omega 3} = 0.4$, $\lambda_{\Omega 4} = 0.75$ and $l_{w0} = 1$, $l_{w1} = 3$, $l_{w2} = 1.2$, $m_w = 1.5$, $n_w = 0.75$, $\lambda_{w1} = 4.5$, $\lambda_{w2} = 3$, $\lambda_{w3} = 0.2$, $\lambda_{w4} = 0.15$. The parameters with respect to the disturbance observers are $\alpha_\Omega = \alpha_w = 3.5$, $k_{\Omega 1} = k_{w1} = 80$, $k_{\Omega 2} = k_{w2} = 0.2$, $p_\Omega = p_w = 3$, $q_\Omega = q_w = 2$. The parameters of integral sliding mode filter are set as $\kappa_{w1} = \kappa_{w2} = 10$, $\sigma_{w1} = \sigma_{w2} = 0.001$, $\mu_{f1} = \mu_{f2} = 0.01$. For brevity, we only present the first 40 seconds simulation results here and assume that just the control output $y = \Omega$ is feasible during the simulation process. Furthermore, the numerical simulations are conducted in MATLAB environment associated with a fixed sampling time 1 ms.

4.2. Results discussions

The simulation results for the aeroservoelastic RLV during reentry phase are provided in Figs. 1-8.

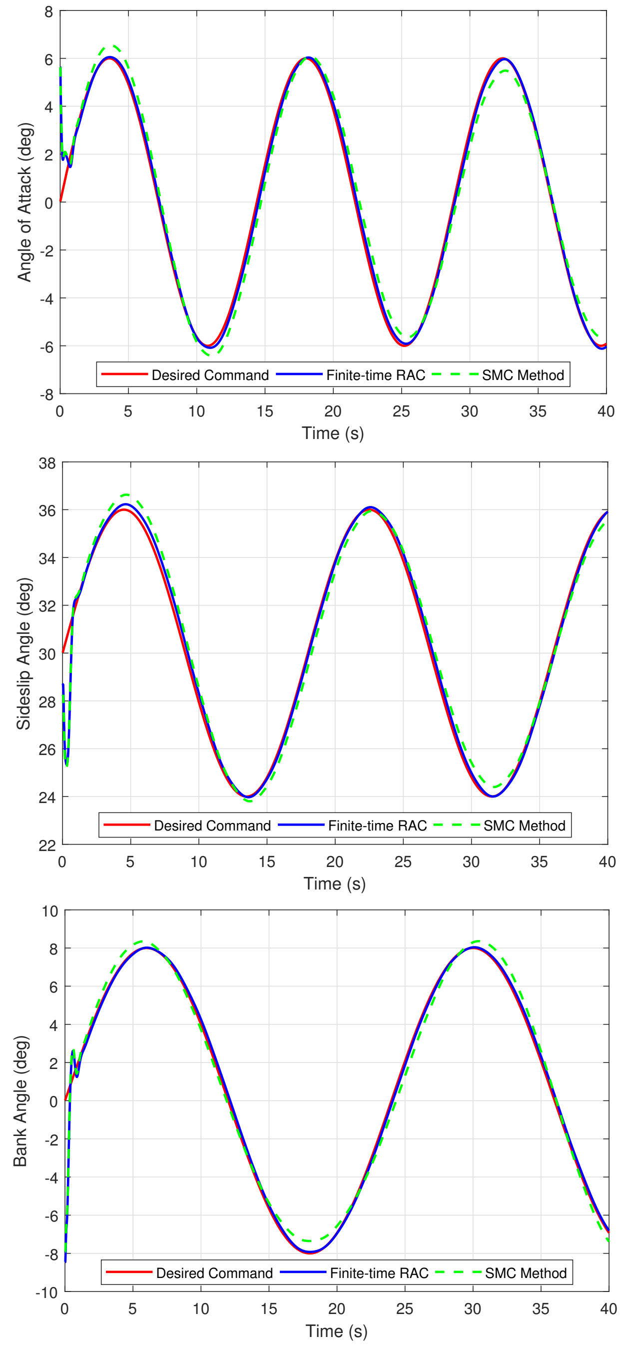

Fig. 1. Tracking curves of attitude angles: AOA, Sideslip Angle and BA.

The tracking curves of attitude angles are presented in Fig. 1. It can be observed clearly that the reentry attitude angles converge to their desired commands quickly within finite-time and the proposed Finite-time RAC scheme shows an favorable tracking performance despite the presence of parameter uncertainties and external disturbances. Similarly, the tracking error curves of attitude angles are shown in Fig. 2. which indicates that the designed control law has higher tracking accuracy than traditional sliding

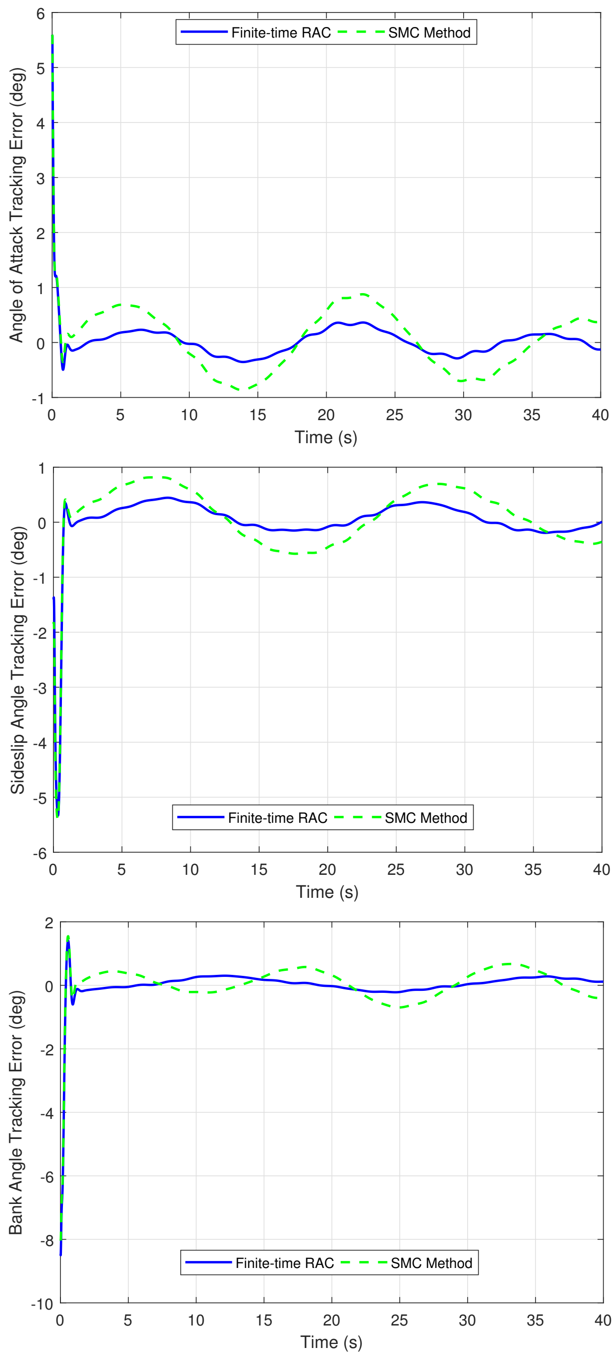

Fig. 2. Tracking error curves of attitude angles: AOA, Sideslip Angle and BA.

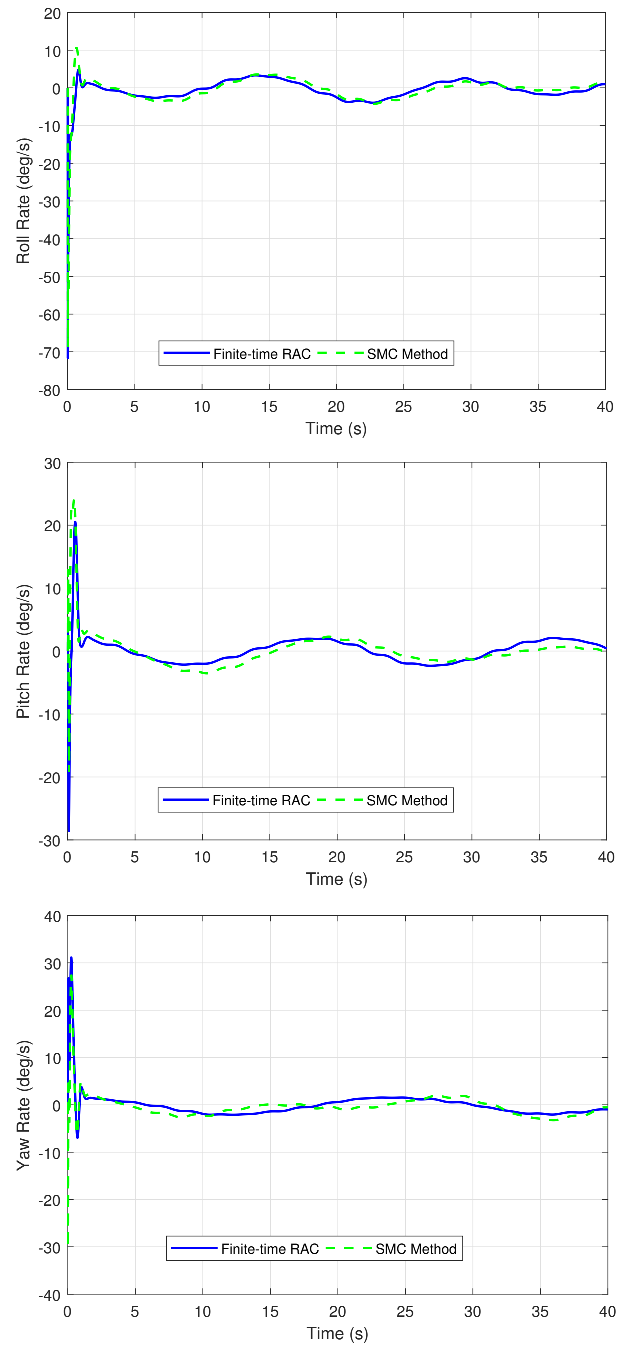

Fig. 3. Responses of angular rates: roll, pitch and yaw rates.

mode control (SMC) approach mainly based on [28].

Figs. 3 and 6 give the responses of angular rates and control moments. The results in Figs. 3 and 6 imply that the angular rates and control moments vary dramatically at the beginning in order to enforce the RLV attitude angles track the desired values in finite time. After that, the angular rates and control moments maintain within the appropriate range. Besides, the estimation values for uncertainty d_Ω and disturbance d_w are shown in Figs. 4 and 5. Obviously, it can be observed that the estimated values of the uncertainty d_Ω and disturbance d_w are effective, while the finite-time convergence of the developed FTSMDO is guaranteed.

Meanwhile, the detailed variations of the elastic coordinates η_1, η_2, η_3 and their derivatives $\dot{\eta}_1$, $\dot{\eta}_2$, $\dot{\eta}_3$ are depicted by Figs. 7 and 8. Following from the graphical data in Figs. 7 and 8, it can be obtained that the elastic coordinate derivatives are able to converge rapidly, while the

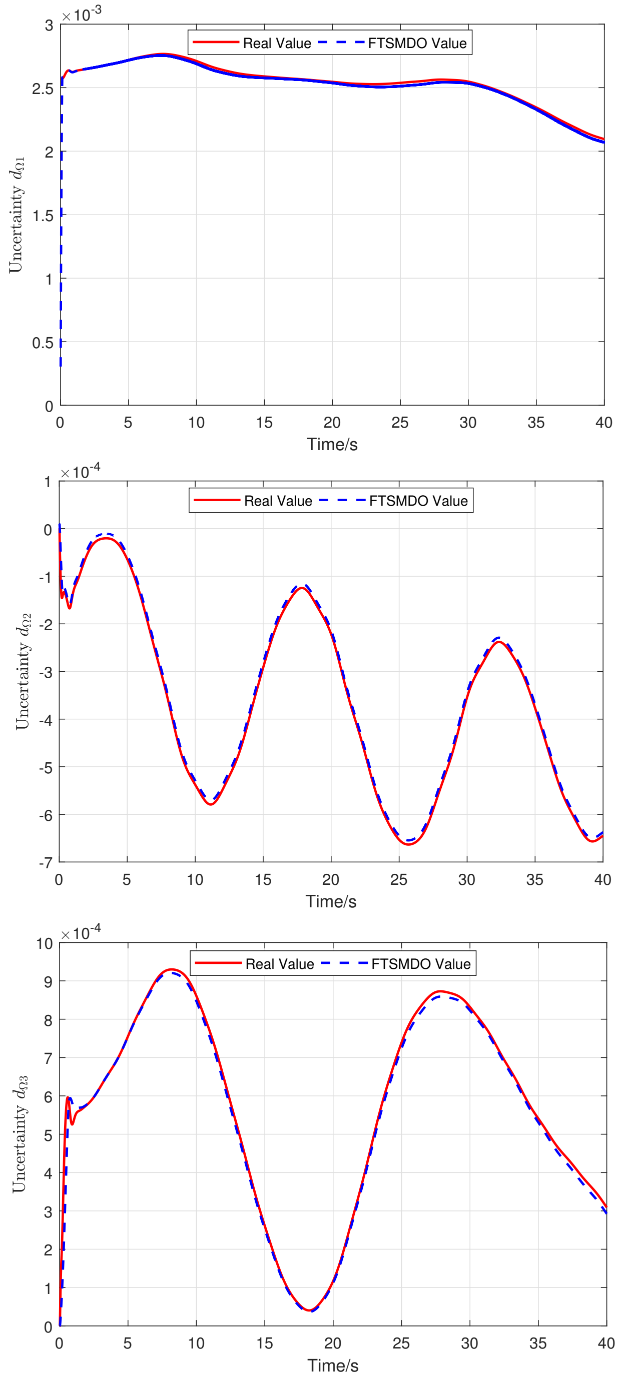

Fig. 4. Curves for uncertainty estimations.

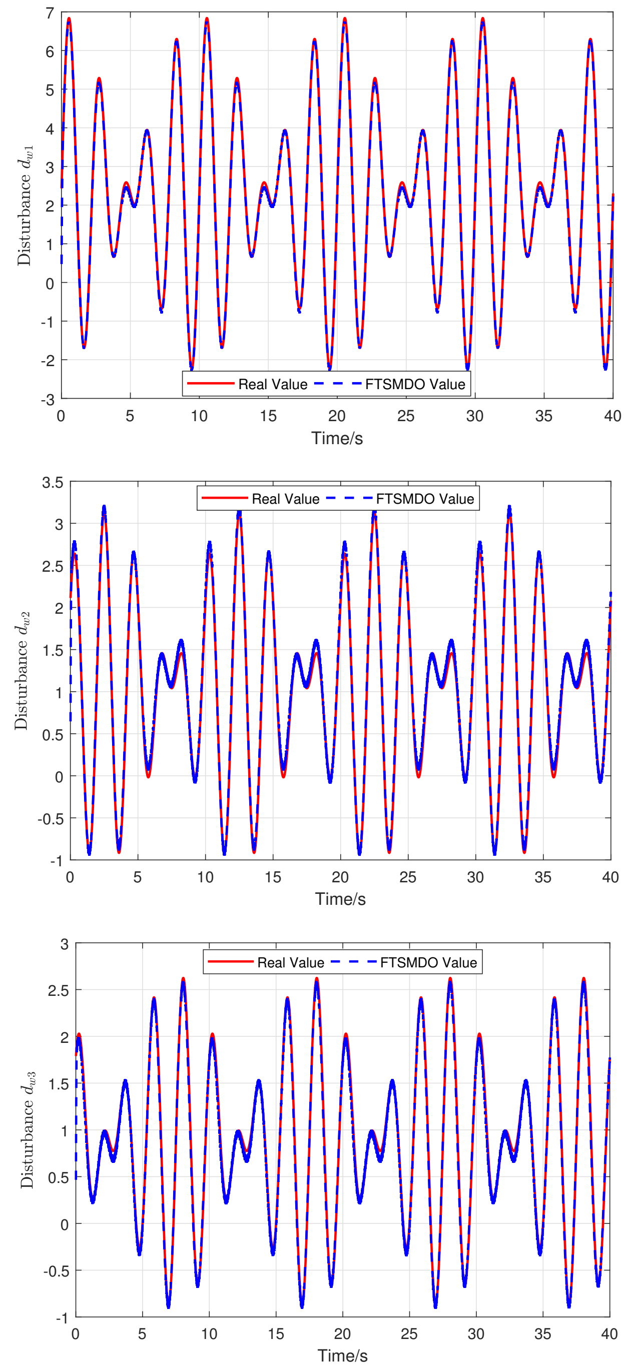

Fig. 5. Curves for disturbance estimations.

elastic coordinate derivatives perform well with rapid convergence. In fact, it is noteworthy that one of main factors of elastic vibration comes from the deflection angles. Thus, Figs. 7 and 8 illustrate that the values of η_1, η_2, η_3 and $\dot{\eta}_1$, $\dot{\eta}_2$, $\dot{\eta}_3$ are large and change quickly at the beginning due to the sudden change of the deflection angles. However, the elastic vibration can decrease evidently in finite time under the developed attitude control strategy.

5. CONCLUSION

A finite-fame design of disturbance observer and reentry attitude controller is developed for aeroservoelastic RLV with parameter uncertainties and external disturbances. The FTSMDO is proposed to provide estimations for the uncertainties and disturbances, where the finite time convergence of estimation errors is guaranteed. And then the finite-time super-twisting sliding mode con-

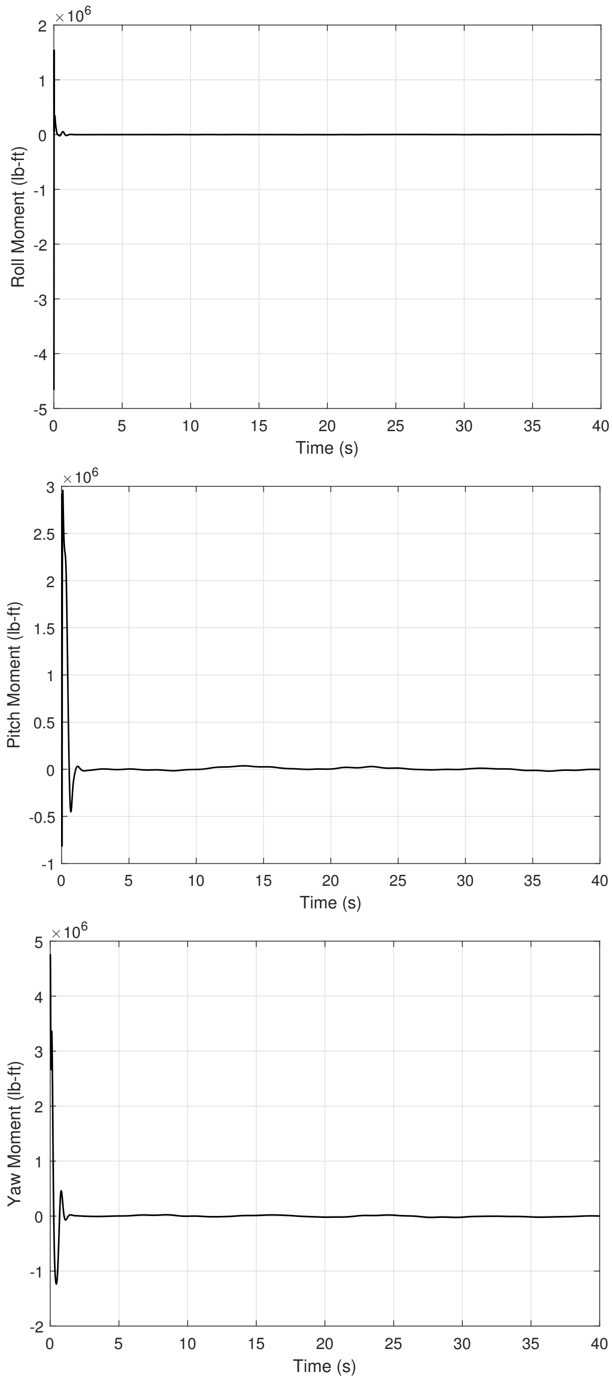

Fig. 6. Responses of control moments.

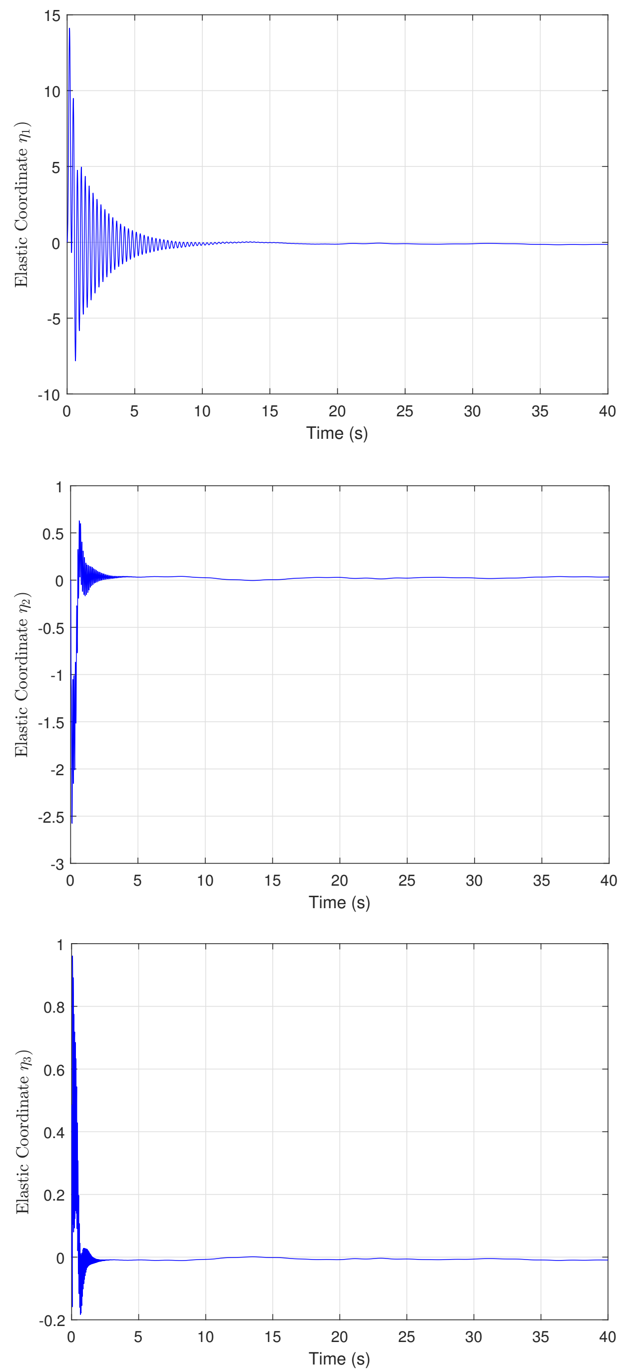

Fig. 7. Responses of elastic coordinates.

trol algorithm is employed to construct reentry attitude controller, which assures that the desired command can be tracked in finite time. Additionally, an integral sliding mode filter with finite time convergence is introduced to deal with the virtual input. Finally, the efficiency of the designed finite-time RAC scheme is verified via numerical simulations.

REFERENCES

[1] Q. Mao, L. Dou, B. Tian, and Q. Zong, "Reentry attitude control for a reusable launch vehicle with aeroservoelastic model using type-2 adaptive fuzzy sliding mode control," *International Journal of Robust and Nonlinear Control*, vol. 28, no. 18, pp. 5858-5875, 2018.

[2] B. Tian, W. Fan, R. Su, and Q. Zong, "Real-time trajectory and attitude coordination control for reusable launch

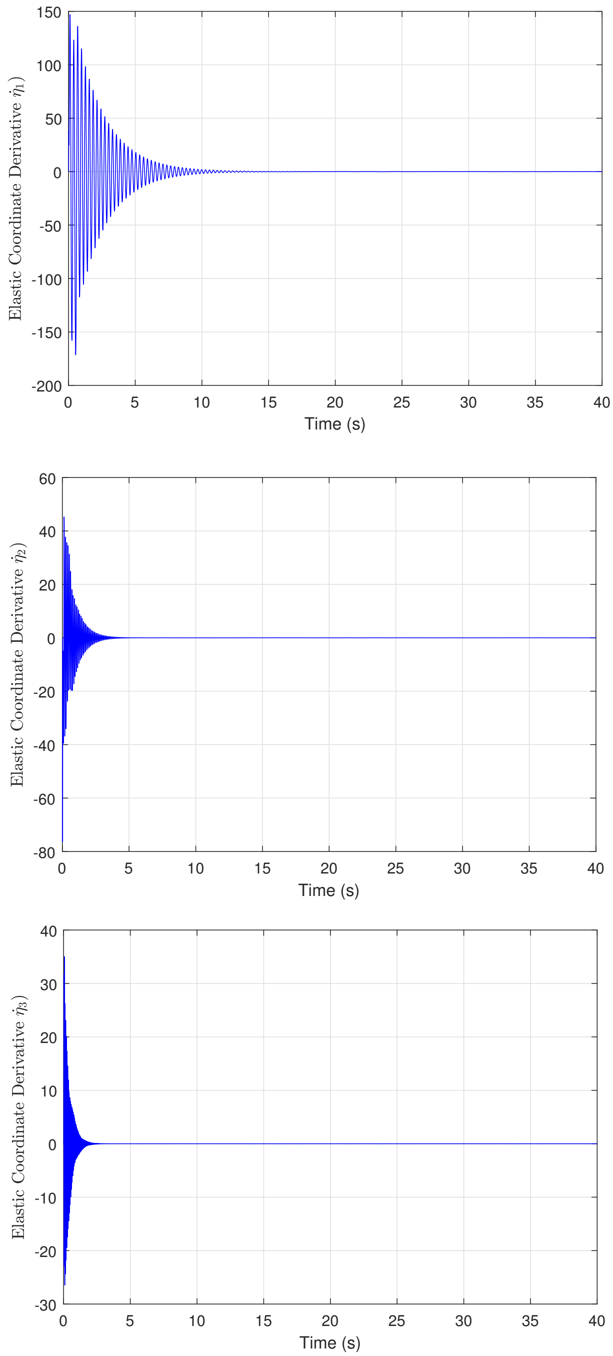

Fig. 8. Responses of elastic coordinate derivatives.

vehicle in reentry phase," *IEEE Transactions on Industrial Electronics*, vol. 62, no. 3, pp. 1639-1650, 2014.

[3] Q. Mao, L. Dou, Z. Yang, B. Tian, and Q. Zong, "Fuzzy disturbance observer-based adaptive sliding mode control for reusable launch vehicles with aeroservoelastic characteristic," *IEEE Transactions on Industrial Informatics*, vol. 16, no. 2, pp. 1214-1223, 2019.

[4] B.-W. Chen and L.-G. Tan, "Adaptive anti-saturation tracking control with prescribed performance for hypersonic vehicle," *International Journal of Control, Automation, and Systems*, vol. 18, no. 2, pp. 394-404, 2020.

[5] X. Lv, Y. Fang, Z. Mao, B. Jiang, and R. Qi, "Fault detection for a class of closed-loop hypersonic vehicle system via hypothesis test method," *International Journal of Control, Automation, and Systems*, vol. 19, no. 1, pp. 350-362, 2021.

[6] J. J. McNamara and P. P. Friedmann, "Aeroelastic and aerothermoelastic analysis in hypersonic flow: Past, present, and future," *AIAA Journal*, vol. 49, no. 6, pp. 1089-1122, 2011.

[7] D. Zhang, S. Tang, Q. Zhu, and R. Wang, "Analysis of dynamic characteristics of the rigid body/elastic body coupling of air-breathing hypersonic vehicles," *Aerospace Science and Technology*, vol. 48, pp. 328-341, 2016.

[8] Y. Peng, H. Yang, Y. Cheng, and B. Jiang, "Largest recoverable component based fault recoverability of UAV swarm with removal of faulty individuals," *Aerospace Science and Technology*, vol. 118, p. 107059, 2021.

[9] R. Ricketts, T. Noll, W. Whitlow Jr., and L. Huttsell, "An overview of aeroelasticity studies for the national aerospace plane," *Proc. of 34th Structures, Structural Dynamics and Materials Conference*, p. 1313, 1993.

[10] F. R. Chavez and D. K. Schmidt, "Analytical aeropropulsive-aeroelastic hypersonic-vehicle model with dynamic analysis," *Journal of Guidance, Control, and Dynamics*, vol. 17, no. 6, pp. 1308-1319, 1994.

[11] M. A. Bolender and D. B. Doman, "Nonlinear longitudinal dynamical model of an air-breathing hypersonic vehicle," *Journal of Spacecraft and Rockets*, vol. 44, no. 2, pp. 374-387, 2007.

[12] X. Hu, L. Wu, C. Hu, and H. Gao, "Adaptive sliding mode tracking control for a flexible air-breathing hypersonic vehicle," *Journal of the Franklin Institute*, vol. 349, no. 2, pp. 559-577, 2012.

[13] Q. Zong, F. Wang, B. Tian, and R. Su, "Robust adaptive dynamic surface control design for a flexible air-breathing hypersonic vehicle with input constraints and uncertainty," *Nonlinear Dynamics*, vol. 78, no. 1, pp. 289-315, 2014.

[14] G. Cheng, W. Jing, and C. Gao, "Recovery trajectory planning for the reusable launch vehicle," *Aerospace Science and Technology*, vol. 117, p. 106965, 2021.

[15] J. Wang, Q. Zong, R. Su, and B. Tian, "Continuous high order sliding mode controller design for a flexible air-breathing hypersonic vehicle," *ISA Transactions*, vol. 53, no. 3, pp. 690-698, 2014.

[16] A. Falcoz, D. Henry, and A. Zolghadri, "Robust fault diagnosis for atmospheric reentry vehicles: A case study," *IEEE Transactions on Systems, Man, and Cybernetics-Part A: Systems and Humans*, vol. 40, no. 5, pp. 886-899, 2010.

[17] L. Fiorentini and A. Serrani, "Adaptive restricted trajectory tracking for a non-minimum phase hypersonic vehicle model," *Automatica*, vol. 48, no. 7, pp. 1248-1261, 2012.

[18] Z. Zuo, J. Song, B. Tian, and M. Basin, "Robust fixed-time stabilization control of generic linear systems with mismatched disturbances," *IEEE Transactions on Systems, Man, and Cybernetics: Systems*, vol. 52, no. 2, pp. 759-768, 2022.

[19] B. Tian, L. Liu, H. Lu, Z. Zuo, Q. Zong, and Y. Zhang, "Multivariable finite time attitude control for quadrotor UAV: Theory and experimentation," *IEEE Transactions on Industrial Electronics*, vol. 65, no. 3, pp. 2567-2577, 2017.

[20] H. An, J. Liu, C. Wang, and L. Wu, "Disturbance observer-based antiwindup control for air-breathing hypersonic vehicles," *IEEE Transactions on Industrial Electronics*, vol. 63, no. 5, pp. 3038-3049, 2016.

[21] M. Sato, "Robust gain-scheduled flight controller using inexact scheduling parameters," *Proc. of American Control Conference*, pp. 6829-6834, IEEE, 2013.

[22] D. Saussié, L. Saydy, O. Akhrif, and C. Bérard, "Gain scheduling with guardian maps for longitudinal flight control," *Journal of Guidance, Control, and Dynamics*, vol. 34, no. 4, pp. 1045-1059, 2011.

[23] W. van Soest, Q. Chu, and J. Mulder, "Combined feedback linearization and constrained model predictive control for entry flight," *Journal of Guidance, Control, and Dynamics*, vol. 29, no. 2, pp. 427-434, 2006.

[24] O. Ur Rehman, I. R. Petersen, and B. Fidan, "Feedback linearization-based robust nonlinear control design for hypersonic flight vehicles," *Proceedings of the Institution of Mechanical Engineers, Part I: Journal of Systems and Control Engineering*, vol. 227, no. 1, pp. 3-11, 2013.

[25] Z. Su and H. Wang, "A novel robust hybrid gravitational search algorithm for reusable launch vehicle approach and landing trajectory optimization," *Neurocomputing*, vol. 162, pp. 116-127, 2015.

[26] C. Mu, Z. Ni, C. Sun, and H. He, "Air-breathing hypersonic vehicle tracking control based on adaptive dynamic programming," *IEEE Transactions on Neural Networks and Learning Systems*, vol. 28, no. 3, pp. 584-598, 2016.

[27] L. Ye, B. Tian, H. Liu, Q. Zong, B. Liang, and B. Yuan, "Anti-windup robust backstepping control for an underactuated reusable launch vehicle," *IEEE Transactions on Systems, Man, and Cybernetics: Systems*, vol. 52, no. 3, pp. 1492-1502, 2022.

[28] Y. Shtessel, C. Hall, and M. Jackson, "Reusable launch vehicle control in multiple-time-scale sliding modes," *Journal of Guidance, Control, and Dynamics*, vol. 23, no. 6, pp. 1013-1020, 2000.

[29] C. E. Hall and Y. B. Shtessel, "Sliding mode disturbance observer-based control for a reusable launch vehicle," *Journal of Guidance, Control, and Dynamics*, vol. 29, no. 6, pp. 1315-1328, 2006.

[30] J. E. Stott and Y. B. Shtessel, "Launch vehicle attitude control using sliding mode control and observation techniques," *Journal of the Franklin Institute*, vol. 349, no. 2, pp. 397-412, 2012.

[31] Z. Wang, W. Bao, and H. Li, "Second-order dynamic sliding-mode control for nonminimum phase underactuated hypersonic vehicles," *IEEE Transactions on Industrial Electronics*, vol. 64, no. 4, pp. 3105-3112, 2016.

[32] Q. Zong, J. Wang, B. Tian, and Y. Tao, "Quasi-continuous high-order sliding mode controller and observer design for flexible hypersonic vehicle," *Aerospace Science and Technology*, vol. 27, no. 1, pp. 127-137, 2013.

[33] Q. Mao, L. Dou, Q. Zong, and Z. Ding, "Attitude controller design for reusable launch vehicles during reentry phase via compound adaptive fuzzy H-infinity control," *Aerospace Science and Technology*, vol. 72, pp. 36-48, 2018.

[34] B. Xu, X. Wang, and Z. Shi, "Robust adaptive neural control of nonminimum phase hypersonic vehicle model," *IEEE Transactions on Systems, Man, and Cybernetics: Systems*, vol. 51, no. 2, pp. 1107-1115, 2021.

[35] L. Dou, M. Du, Q. Mao, and Q. Zong, "Finite-time nonsingular terminal sliding mode control-based fuzzy smooth-switching coordinate strategy for AHV-VGI," *Aerospace Science and Technology*, vol. 106, p. 106080, 2020.

[36] W. Yang, D. Xu, B. Jiang, and P. Shi, "A novel dual-mode robust model predictive control approach via alternating optimizations," *Automatica*, vol. 133, p. 109857, 2021.

[37] Y. Hong, J. Wang, and D. Cheng, "Adaptive finite-time control of nonlinear systems with parametric uncertainty," *IEEE Transactions on Automatic control*, vol. 51, no. 5, pp. 858-862, 2006.

[38] S. Li, S. Ding, and Q. Li, "Global set stabilisation of the spacecraft attitude using finite-time control technique," *International Journal of Control*, vol. 82, no. 5, pp. 822-836, 2009.

[39] B. Tian, J. Cui, H. Lu, Z. Zuo, and Q. Zong, "Adaptive finite-time attitude tracking of quadrotors with experiments and comparisons," *IEEE Transactions on Industrial Electronics*, vol. 66, no. 12, pp. 9428-9438, 2019.

[40] B. Tian, J. Cui, H. Lu, L. Liu, and Q. Zong, "Attitude control of UAVs based on event-triggered supertwisting algorithm," *IEEE Transactions on Industrial Informatics*, vol. 17, no. 2, pp. 1029-1038, 2020.

[41] S. Yu, X. Yu, B. Shirinzadeh, and Z. Man, "Continuous finite-time control for robotic manipulators with terminal sliding mode," *Automatica*, vol. 41, no. 11, pp. 1957-1964, 2005.

[42] Y.-S. Lu, "Sliding-mode disturbance observer with switching-gain adaptation and its application to optical disk drives," *IEEE Transactions on Industrial Electronics*, vol. 56, no. 9, pp. 3743-3750, 2009.

[43] J. A. Moreno and M. Osorio, "A Lyapunov approach to second-order sliding mode controllers and observers," *Proc. of 47th IEEE Conference on Decision and Control*, IEEE, pp. 2856-2861, 2008.

Zhenshu Yang received her B.S. degree in electrical engineering and automation from the Tianjin University of Science and Technology, Tianjin, China, in 2015, and an M.S. degree in the aeronautical and astronautical science and technology from the Civil Aviation University of China, Tianjin, China, in 2018, respectively. She is currently a lecturer in the Aeronautical Engineering Institute, Jiangsu Aviation Technical College. Her current research interests are in the fields of fault diagnosis and detection, and flight control system design.

Qi Mao received his B.S. degree in electrical engineering and automation from the Tianjin University of Science and Technology, Tianjin, China, in 2015, and an M.S. degree in the control science and engineering from the Tianjin University, Tianjin, China, in 2018, respectively. He is currently working toward a Ph.D. degree in the Department of Electrical Engineering, City University of Hong Kong, Kowloon, Hong Kong. His current research interests include PID control, time-delay systems, multiagent systems, and flight control.

Liqian Dou received his B.S., M.S., and Ph.D. degrees in automatic control from Tianjin University, Tianjin, China, in 1999, 2005, and 2008, respectively. He was an Academic Visitor in the School of Electrical and Electronic Engineering, University of Manchester, Manchester, U.K., from June 2015 to June 2016. He is currently an Associate Professor in the School of Electrical and Information Engineering, Tianjin University, Tianjin, China. His main research interests include nonlinear control for hypersonic vehicle, attitude control for RLV, and coordinate control of multi-UAVs.

Qun Zong received his Bachelor's, Master's and Ph.D. degrees all in automatic control from Tianjin University, Tianjin, China, in 1983, 1988, and 2002, respectively. He is currently a professor at the School of Electrical and Information Engineering, Tianjin University. His main research interests include complex system modeling and flight control.

Jianzhong Yang received his Bachelor's and Master's degrees in power electronics and power drives from Liaoning Technical University, Liaoning, China, in 1997 and 2000, respectively. He is currently a professor at the College of Electrinic Information and Automation, Civil Aviation University of China. His main research interests include civil aircraft system safety analysis and assessment, and advanced flight control.